Hindawi
Advances in Civil Engineering
Volume 2020, Article ID 9490807, 18 pages
https://doi.org/10.1155/2020/9490807

Research Article

Study of the Rock Crack Propagation Induced by Blasting with a Decoupled Charge under High In Situ Stress

Xudong Li, Kewei Liu, and Jiacai Yang

School of Resources and Safety Engineering, Central South University, Changsha 410083, China

Correspondence should be addressed to Kewei Liu; kewei_liu@csu.edu.cn

Received 27 September 2019; Revised 26 November 2019; Accepted 9 January 2020; Published 10 March 2020

Academic Editor: Roberto Nascimbene

The high in situ stress can significantly affect the blast-induced rock fragmentation and cause difficulties in deep mining and civil engineering where the drilling and blasting technique is applied. In this study, the rock crack propagation induced by blasting under in situ stress is first analyzed theoretically, and then a numerical model with a decoupled charge in LS-DYNA is developed to reveal how the initiation and propagation of rock cracks are under high in situ stress. Through simulation, the mechanisms of blast-induced crack evolution under various hydrostatic pressures and nonhydrostatic pressures are investigated, and the differences in crack evolution with specific decoupling coefficients are compared. According to the simulation, three damage zones, i.e., the crushed zone, the nonlinear fracture zone, and the radial crack propagation zone, are formed, and the radial crack evolution is greatly suppressed by the high in situ stress which has no much influence on the crack propagation in the crushed and the nonlinear fracture zones. The velocity of crack propagation is slightly reduced, and the process of crack propagation is stopped early when the rock is subjected to high in situ stress. Furthermore, the numerical analysis indicates that the crack grows preferentially in the direction of maximum principal stress, and the radial crack propagation is predominantly controlled by the preloaded pressure, which is vertical to the crack propagation direction. Based on the numerical results, it is suggested that the optimal decoupling coefficients for rock cracking are 2.65, 1.87, 1.37, and 1.22 for 0, 10, 20, and 30 MPa, respectively. This study provides not only an analysis of the rock crack evolution under high in situ stress but also a reference for resolving excavation difficulties in deep mining.

1. Introduction

With the depletion of shallow-buried mineral resources, mining has a tendency of extending to great depth. Following the increase in depth, the rock mass is under a continuously increased stress condition. For instance, TauTona gold mine of South Africa, the deepest mine in the world, is currently operating at a depth more than 4000 m [1] and the in situ stress is about 100 MPa at the level of 3500 m [2]. In deep mining, the drilling and blasting (D&B) method is widely used for rock excavation. The rock fragmentation by blasting is the first stage of the comminution process in mine, and it affects every downstream operation, such as digging, hauling, crushing, and grinding; therefore, it is vital for the efficiency of deep mining operation [3, 4]. When the rock mass is subjected to high in situ stress, the rock fragmentation by blasting is impeded by high in situ stress [4–6], and several issues, such as underbreak and oversize fragmentation, can be aroused. To response this situation, it is essential to study the rock fracturing by blasting with the aim of expected rock fragmentation when the rock mass is subjected to high in situ stress.

Many studies have been done in the field of rock crack initiation and propagation induced by blasting under preexisting stress. In 1971, Kutter and Fairhurst [7] studied the dynamic fracture of rock discs induced by blast loading under uniaxial static stress. The obtained cracks in the experiment demonstrated that the crack propagation aligns with the direction of applied static stress, and some of the cracks, which initiated in a radial direction other than that of the static stress field, eventually curved off into the direction of the applied pressure. Rossmanith et al. [8] investigated the

fracturing mechanism under dynamic-static loading with explosion and preloaded pressure on three-dimensional cube-type rock-like material (polymethyl methacrylate), and the test results showed that the fracture preferentially propagates in the direction of the major principal stress. Yang et al. [9] researched the mechanism of rock crack propagation under static stress and blast loading by means of caustics experiment, and the results indicated that the preloaded pressure which is vertical to the direction of crack propagation reduces the stress intensity factor at the crack tip and thus suppresses the propagation of cracks. In Yang's further work [10], it was pointed out that the maximum tensile stress is generated in the direction of the maximum principal stress of the borehole, and the combination of the initial static stress and blast loading causes the longest rock crack to propagate preferentially in the direction of initial static stress field.

Besides laboratory experiments, many theoretical analyses were also conducted for achieving the optimal fragmentation by blasting, which provide the predictions of fragmentation with different rock types, blasting patterns, and explosive parameters [3]. Considering the preexisting stress, a theoretical model for predicting the propagation of blast-induced rock cracks was firstly proposed by Nilson et al. [11] in 1985, and the accuracy of the theoretical model was verified with experimental data from the Sandia National Laboratory [12–14]. Improved model for a cylindrical borehole in a static stress field with radical cracks was put forward by Paine and Please [15] in 1994, and it was applied to predict the process of blast-induced dynamic crack propagation and the rapid pressure reduction in borehole under in situ stress. At the same year, inspired by the work of Nilson et al. [11], Lu and Tao [16] developed a crack propagation model by analyzing and calculating the stress intensity factor at the crack tip to solve the velocity of crack propagation induced by explosion products theoretically. This model was further applied by Lu et al. [17] and Hu et al. [18] to predict the attenuation process of detonated gas pressure within cracks and the propagation of presplit cracks under in situ stress. These theoretical studies are very meaningful for comprehending the mechanisms of blast-induced crack initiation and propagation under in situ stress; however, they still have some shortcomings owing to several simplicities in the theoretical analysis, and the precision of predicting rock fragmentation is limited due to the lack of understanding of the complexity of the blasting process [19]. The vital need for better understanding of the dynamic rock fracturing process in blasting was particularly highlighted in the excellent review works by Latham et al. [20], Saharan et al. [21], and An et al. [3]. Therefore, further study of the mechanism of rock fracturing and crack propagation under high in situ stress is extremely necessary.

In conjunction with the development of computer power, topological data structure, and commercial hydrocodes, the numerical method has been a widely used tool to study blast-induced rock damage or cracking. The finite element method (FEM) could be the most common approach for numerical analysis in rock blasting. Preece and Thorne [22] used the 3D finite element technique with a damage constitutive model to study the effect of detonation-timing on rock fragmentation. Bendezu et al. [23] presented a numerical analysis to simulate blast-induced hard rock fracture propagation. In their study, three different methods, i.e., the extended finite element method, the conventional finite element method, and the element deletion method, were compared in their paper to simulate rock fragmentation. Besides the finite element method, the discrete element method (DEM) and combined finite-discrete element method (FEM-DEM) are also popular for simulating rock fracturing under blasting [24–32]. Preece and Chung [33] developed an algorithm to analyze some unnatural behaviour of discrete elements during the formation of muck pile subsequent to explosive loading. Owen et al. [34] used the combined finite-discrete element method to model blast-induced rock failures. Munjiza [26] investigated the fracture and fragmentation patterns of bench blasting by employing the hybrid finite-discrete element method. These works in the field of computational modelling of blasting operations are pretty meaningful for understanding the mechanic of blast-induced rock cracking. More excellent works on the numerical modelling of rock blasting can be found in reviews of Latham and Lisjak [35, 36]. At present, many numerical studies [4–6, 37–41] in investigating the fracturing mechanism of rock under blast loading and in situ stress have been performed. In 1997, Donze et al. [41] developed a numerical model based on the discrete element method to investigate the effect of stress waves on the initiation and propagation of radial cracks in an uniaxial static stress field during the dynamic loading phase of an explosion. The results showed that the cracks align along the main stress axis. Ma and An [38] used a 2D finite element model to study the effect of static stress field on the propagation of blasting-induced cracks. The simulation results showed that the in situ stress suppresses the propagation of rock cracks and cracks and preferentially propagates in the direction of the maximum principal stress. Yilmaz and Unlu [40] established a 3D numerical model based on the finite difference method to study the effects of the direction and the magnitude of the maximum principal stress on the development of the cracks around the borehole, and the results indicated that the cracks initiate radially but finally tend to develop parallel to the direction of the maximum principal stress. Xie et al. [5] developed a tension and compression-shear damage model and applied it in the mechanism analysis of cut blasting damage evolution in deep tunnel rock. The research results indicated that the high in situ stress has resistance on the radially oriented detonation pressure and the damage extension around boreholes. In the further study of Xie et al. [6], the numerical analysis revealed that the coalescence of blast-induced cracks between adjacent boreholes becomes difficult when the in situ stress is higher than 30 MPa. Inspired by the above numerical studies, Yi et al. [4] investigated the rock fracture patterns of full charged borehole under various in situ stress conditions, and the results showed that the crack propagation in the

vicinity of the blasthole is controlled by the blast loading, while it is suppressed by the high in situ stress in the far-field. These numerical investigations mentioned above provide good insights about the effect of in situ stress on the rock crack evolution due to blast loading. However, in these studies, the blast loading was usually represented by a pressure-time history curve [37–41], which cannot accurately characterize the detonation of explosive [4]. Furthermore, the boreholes were fully charged [4–6], and this is not always in line with the practices of deep rock blasting. In fact, in deep mining, the charging in a number of boreholes is decoupled, especially in presplit blasting, smooth blasting, buffer blasting, and some production blasting [42–44], but few papers can be found to study the rock fracturing in blasting with a decoupled charge under high in situ stress.

In this study, the rock crack propagation induced by blasting under in situ stress is firstly analyzed theoretically, and then a numerical model with a decoupled charge in the LS-DYNA code is developed to investigate the crack evolution of rock mass subjected to coupled static stress and blast loading. Through simulation, the mechanisms of blast-induced crack evolution under various hydrostatic and nonhydrostatic pressures are investigated, and the differences in rock fracturing under high in situ stress with different decoupling coefficients are also compared and analyzed. This study provides not only an analysis of the crack evolution under high in situ stress but also a reference for resolving excavation difficulties in deep mining.

2. Theoretical Analysis for Blast-Induced Crack Propagation

It is well known that, in rock blasting, two basic forms of energy, i.e., the shock wave energy and the gas energy, are released [40]. During the blasting, explosion shock waves are generated immediately and they travel outwards from the coupling medium or borehole followed by a longer duration gas pressure. Furthermore, it has been revealed that the explosion shock waves are responsible for the formation of the crushed zone and the initiation of surrounding radial cracks, while the gas pressure further extends these cracks [3, 7, 19, 39, 40, 45]. Kutter and Fairhurst [7] divided the blast-induced rock fragmentation process into four consecutive stages. This division has been extensively accepted, and it is briefly introduced here for offering a comparison with the latter numerical results, which will be presented in Section 4.1.

Figure 1 shows the sketch of the consecutive stages in the cracking process of rock blasting. When the strong shock waves propagate away from the coupling medium or the wall of borehole, the rock in the vicinity of the borehole is immediately fully crushed with relatively uniform and smallest particle size, and the first zone; i.e., the strong-shock (hydrodynamic) zone [7] or the crushed zone [3, 4, 38, 40, 41] (Stage 1) is formed (in some literatures, although the divisions of the consecutive stages of blast-induced rock fragmentation process are same, they are different in the nomenclature of the damage zones). Then, the shock waves pass through the second zone, i.e., the transitional and nonlinear zones [7] or the cracked zone [3] where the rock is severely fractured, but the particle size is rapidly increasing as the increase of radial distance (Stage 2). Thereafter, because of the tensile stress component of the propagating stress wave, radial cracks extend from the edge of the transitional and nonlinear zones and propagate in the third zone, i.e., the elastic zone [7] or the fragment formation zone [21] (Stage 3). Finally, the high-pressure gas promotes the propagation of the cracks; i.e., the crushed zone and the transitional and nonlinear zones are expanded, and the radial cracks are further developed due to the penetration of the high-pressure gas into the cracks (Stage 4).

For a continuous cylindrical charge hole which is subjected to in situ stress, a simplified 2D theoretical model was proposed by Nilson et al. [11] to predict the propagation of blast-induced cracks in a cross section of the cylindrical borehole and rock mass. In this model, it is assumed that the crack propagation is stably driven by quasistatic gas pressure, after the cracked zone is generated by explosion stress waves. The opening displacement of crack is calculated using linear elastic theory, and the inelastic response areas are assumed in small regions including the crack tips and in the vicinity of the borehole. Figure 2 shows the schematic diagram of the planer wedge-shaped crack propagation model, which is subjected to in situ stress. σ is the in situ stress; R is the radius of the borehole; L_0 is the initial length of the crack which is induced by explosion stress waves, and it is set to be $3R$ according to the study of Persson et al. [46]; and $L(t)$ is the total length of crack induced by explosive stress waves and detonation gas.

The detonation gas flow can be modeled in an averaged system that allows the turbulent momentum loss and considers the gas to expand adiabatically [47]. It is assumed to be uniform distribution along the length of the crack and equals the pressure in the borehole [17]. The detonation gas pressure can be characterized using the polytropic equation of state for gas as

$$P(t) = P_0\left(\frac{V_0}{V(t)}\right)^{\gamma}, \tag{1}$$

where $V(t)$ is the total volume of the cracks and borehole, V_0 is the initial volume of the borehole, P_0 is the initial average pressure on the borehole wall, and γ is a constant to control the adiabatic attenuating process of the gas pressure and set to be in the range of 1.2–3.0 [15]. When the charge in borehole is decoupled, the gas pressure exerting on the borehole wall instantaneously rises to its peak [7]. At the same time, the larger the gap between the borehole wall and charge is, the lower the peak pressure will be. This is the principal effect of "decoupled charge" in presplitting or smooth-wall blasting. The initial pressure of explosion gas can be obtained from the Chapman–Jouguet model of detonation pressure [48] as

$$P_0 = \frac{\rho_e D^2}{2(1+\gamma)}\left(\frac{d_e}{d_b}\right)^{2\nu}, \tag{2}$$

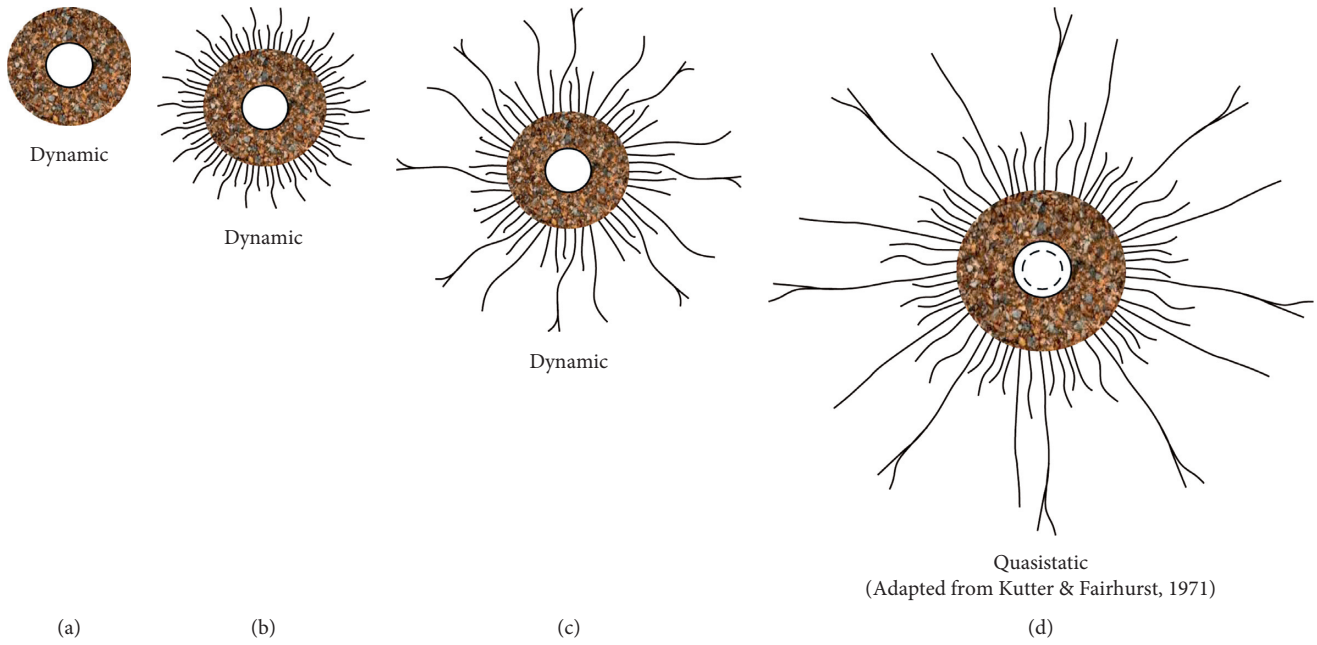

Figure 1: Consecutive stages in the cracking process of rock blasting [7]: (a) crushing zone; (b) crushing and fracture in the nonlinear zone; (c) radial cracks from an elastic wave; (d) expansion of cavity, extension of nonlinear crushed zone, and growth of radial fractures.

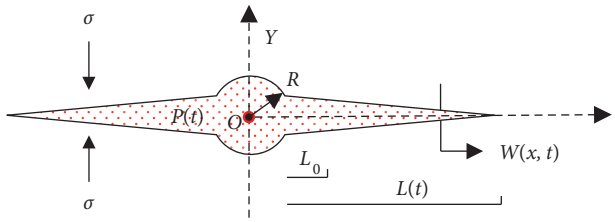

Figure 2: Planer wedge-shaped crack propagation model [11].

where ρ_e is the density of explosive, D is the detonation velocity, d_e is the diameter of explosive, and d_b is the diameter of the borehole. ν is the ratio of specific heats for detonation gas, usually being 1.4.

The condition of stable propagation of a crack in rock mass by gas penetration can be described as

$$K_I(t) > K_{\mathrm{ID}}, \tag{3}$$

where $K_I(t)$ is the stress intensity factor at the crack tip and K_{ID} is the dynamic fracture toughness of rock. The gas cracking of rock mass is a mobile-equilibrium process, which can be expressed using the following balance [49]:

$$\int_0^{L(t)} \frac{P(x,t)-\sigma}{\left[L(t)^2 - x^2\right]^{1/2}}\mathrm{d}x = \frac{1}{2}\sqrt{\frac{\pi}{L(t)}}K_{\mathrm{ID}}, \tag{4}$$

where $P(x,t)$ is the detonation gas-pressure distribution within the crack. In previous theoretical studies [11, 15–17], K_{ID} is usually set as a constant of rock, but actually, it is a variable and has a linear relationship with loading rate. According to the researches on rock dynamic cracking under various loading rates [50–55], the dynamic fracture toughness of rock under blast loading can be written as

$$K_{\mathrm{ID}} = K\frac{\partial(P(x,t))}{\partial t} + K_{\mathrm{IC}}, \tag{5}$$

where K_{IC} is the static fracture toughness of rock and it is 1.8 MPa·m$^{1/2}$ for Barre granite [56]. K is the slope of K_{ID} versus loading rate. In the blasting, cracks initiate from the borehole wall where $x = R$ and propagate to a distance of $x = L(t) + R$, and the stress intensity factor at the crack tip can be calculated as

$$K_I(t) = 2\left[\frac{L(t)+R}{\pi}\right]^{1/2}\int_R^{L(t)+R}\frac{P(x,t)-\sigma}{\left\{[L(t)+R]^2 - x^2\right\}^{1/2}}\mathrm{d}x - K\frac{\partial(P(x,t))}{\partial t}, \tag{6}$$

where $L(t) = \int_0^t C_f(t)\mathrm{d}t$, $C_f(t)$ is the propagation velocity of the crack, and $C_f(t)$ is set to be 0.38 C_p according to the work of Lawn and Wilshaw [57]. C_p is the longitudinal wave velocity of the rock mass. Then, the process of crack propagation under the combination of static stress and blast loading can be calculated with equations mentioned above.

Figure 3(a) shows the results of crack lengths under various in situ stresses obtained by theoretical calculations, in which the hole diameter d_b is 100 mm and the P-wave velocity C_p in Barre granite is 4535 m/s. It indicates that the crack length decreases with the in situ stress increasing, and the decrement of crack length in per MPa declines with the increase in in situ stress. Figure 3(b) shows that the blast-induced crack propagates stably, and the crack evolution stops at different times under different in situ stress due to the stress intensity factor at the crack tip below the dynamic fracture toughness of rock. It should be noted here that

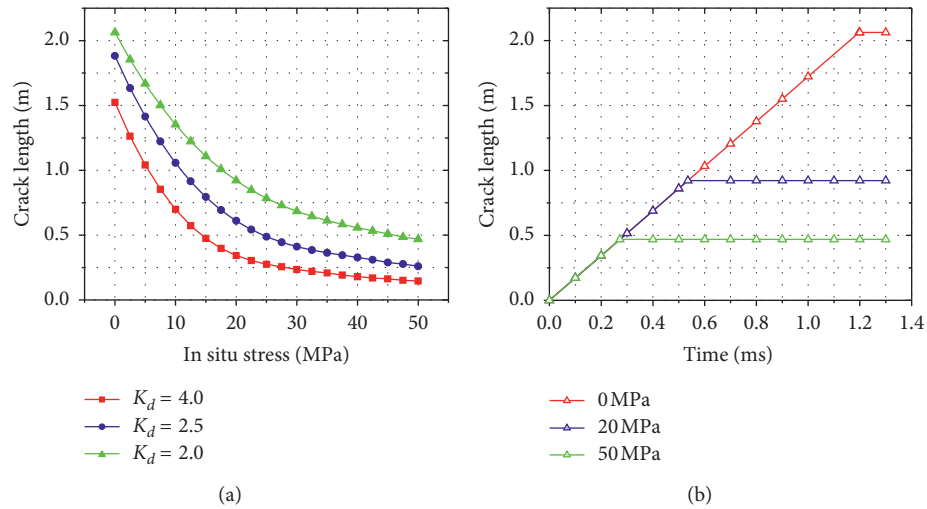

FIGURE 3: Theoretical calculation results: (a) crack lengths under various in situ stresses; (b) crack length-time curves at $K_d = 2.0$ (K_d is the decoupling coefficient, which is defined as the ratio of the borehole diameter to explosive diameter).

because it is difficult to obtain an analytical solution for nonlinear rock mass under blast loading, all these results are based on the assumption that the most domain of rock mass is linear elastic. As a result, error inevitably accumulates gradually during the calculation. Furthermore, for simplification, only main influence factors about rock blasting are considered in theoretical analysis. To respond this situation, it is more reasonable to investigate the dynamic cracking mechanism of nonlinear rock mass in blasting with the means of numerical modelling. Therefore, for the later analysis, numerical simulation is adopted to calculate the propagation of blast-induced rock crack under high in situ stress.

3. Numerical Model and Verification

3.1. Numerical Model. For the accuracy of simulation, numerical calibration is first carried out here based on the laboratory experiment conducted by Banadaki [58]. In his experiment, a 144 mm diameter cylindrical granitic sample with a 6.45 mm diameter centre hole was employed to study the blast-induced rock crack pattern. The obtained crack pattern was mapped by using dye impregnation and digital photography under a high-intensity UV light. Details of the experiment can be found in [58, 59]. Figure 4 shows a 2D plane model, which is built to simulate the crack pattern in the cross section of the cylindrical test sample. It has the same size as the physical model, and the total number of elements is 19352. This numerical model consists of five materials: PETN dynamite, resin, air, copper, and Barre granite. The multi-material ALE method (ALE_MULTI-MATERIAL_GROUP) is used to solve the problem of large deformation in rock blasting simulation. The material models for rock, explosive, and air are listed as follows, respectively.

3.1.1. Material Model for Rock. For the present study, the Riedel–Hiermaier–Thoma (RHT) model, a macro-scale material model proposed by Riedel et al. [60, 61], is chosen for rock. It defines strength characteristics by three limit surfaces, i.e., the inelastic yield surface, the failure surface, and the residual surface. It considers the influence factors of rock mechanical performance in blasting under high in situ stress, including confining pressure, strain rate, strain hardening, and damage softening [62]. The parameters for the RHT material model are determined through a parametric study which is conducted to adjust the appropriate values by comparing the numerical result with the test data. The RHT material parameters for rock are given in Table 1.

3.1.2. Material Model for Explosive. The Material Type 8 of ∗MAT_HIGH_EXPLOSIVE_BURN in LS-DYNA library combined with the Jones–Wilkens–Lee (JWL) equation-of-state (EOS) [63] is chosen to describe the pressure generated by the expansion of the detonation product. It has been widely applied in the calculations of rock blasting [64–66]. The JWL EOS is expressed as

$$P = A\left(1 - \frac{\omega}{R_1 V}\right)e^{-R_1 V} + B\left(1 - \frac{\omega}{R_2 V}\right)e^{-R_2 V} + \frac{\omega E}{V}, \quad (7)$$

where P is the detonation pressure, V is the relative volume of detonation product, E is the internal energy of explosive, and A, B, C, R_1, R_2, and ω are explosive constants. According to Banadaki's experiment [58], the material parameters for explosive are as follows: $A = 5.86 \times 10^2$ GPa, $B = 21.6$ GPa, $R_1 = 5.81$, $R_2 = 1.77$, $\omega = 0.282$, and $E_0 = 7.38$ GPa. The detonation velocity and the density of explosive are 6690 m/s and 1320 kg/m^3, respectively.

3.1.3. Material Model for Air. As for air, material type 9 (∗MAT_NULL) of LS-DYNA library is used together with the EOS_LINEAR_POLYNOMIAL. This EOS defines the relationship between pressure, density, and internal energy, and it has the following form:

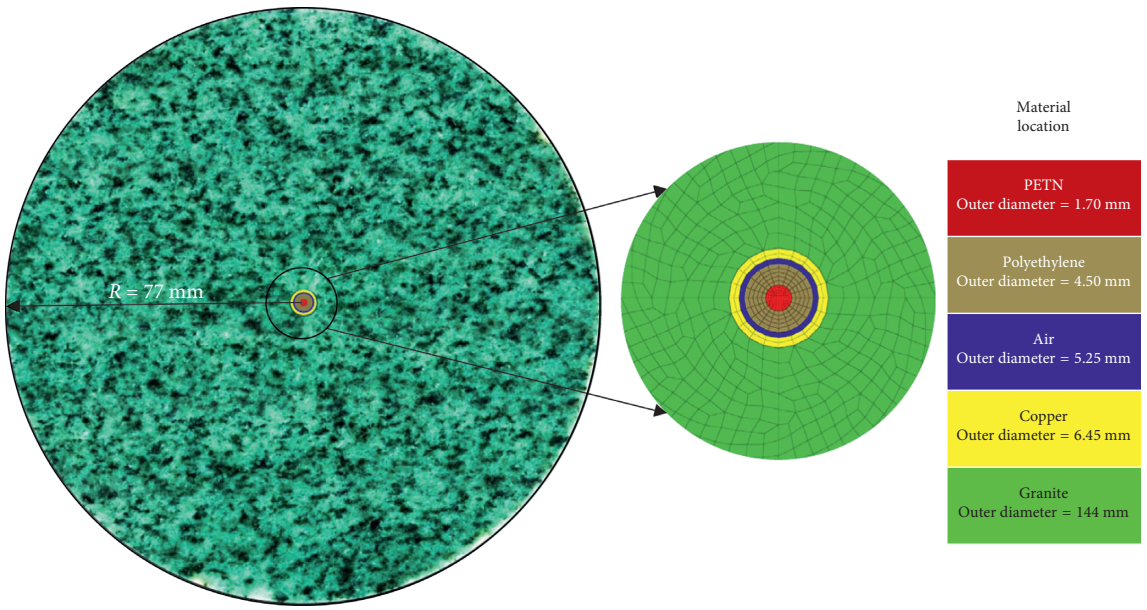

Figure 4: Combination of the model size and material locations.

Table 1: RHT material parameters for rock.

Parameter	Value
Mass density (kg/m^3)	2260
Elastic shear modulus (GPa)	21.9
Eroding plastic strain	2.0
Parameter for polynomial EOS B_0	1.22
Parameter for polynomial EOS B_1	1.22
Parameter for polynomial EOS T_1 (GPa)	25.7
Failure surface parameter A	1.60
Failure surface parameter N	0.61
Compressive strength (MPa)	167.8
Relative shear strength	0.18
Relative tensile strength	0.10
Load angle dependence factor Q_0	0.68
Load angle dependence factor B	0.01
Parameter for polynomial EOS T_2 (GPa)	0.0
Reference compressive strain rate	$3.0E-5$
Reference tensile strain rate	$3.0E-6$
Break compressive strain rate	$3.0E+25$
Break tensile strain rate	$3.0E+25$
Compressive strain rate dependence exponent	0.032
Tensile strain rate dependence exponent	0.036
Volumetric plastic strain fraction in tension	0.001
Compressive yield surface parameter	0.53
Tensile yield surface parameter	0.70
Shear modulus reduction factor	0.50
Damage parameter D_1	0.04
Damage parameter D_2	1.0
Minimum damaged residual strain	0.01
Residual surface parameter AF	1.60
Residual surface parameter NF	0.61
Gruneisen gamma	0.0
Hugoniot polynomial coefficient A_1 (GPa)	35.27
Hugoniot polynomial coefficient A_2 (GPa)	39.58
Hugoniot polynomial coefficient A_3 (GPa)	9.04
Crush pressure (MPa)	125
Compaction pressure (GPa)	6.0
Porosity exponent	3.0
Initial porosity	1.0

$$P = C_0 + C_1\mu + C_2\mu_2 + C_3\mu_3 + (C_4 + C_5 + C_6\mu_2)E, \quad (8)$$

where P is the pressure, E is the internal energy per volume, and μ defines the compression of air by $\mu = (\rho/\rho_0) - 1$ with ρ and ρ_0 being the current and initial density of air, respectively. The air is often modeled by setting $C_0 = C_1 = C_2 = C_3 = C_6 = 0$ and $C_4 = C_5 = \gamma - 1$ with γ being the ratio of specific heats. The standard ratio γ, density ρ_0 of air, and initial internal energy E_0 are 1.4, 1.29 kg/m^3, and 0.25×10^6 J/m^3, respectively.

3.2. Numerical Verification. Figure 5 shows the crack pattern obtained by simulation; when the blast-induced shock waves in the test sample propagate through the coupling medium and borehole wall, the crushed zone and the transitional and nonlinear zones are instantly generated by compression and shear in the vicinity of the borehole (Zone 1). As the shock waves continue to transmit outward, the shock waves gradually attenuate to stress waves. Crushing stops and the radial cracks start to propagate because the tensile stress component exceeds the dynamic tensile strength of rock (Zone 2). When the stress waves arrive at the free surface, the compressive stress waves reflect and change into tensile stress waves. Circumferential spalling cracks therefore appear nearby the free boundary due to the tensile stress waves in the radial direction. At the same time, the tensile stress component exceeds the dynamic tensile failure criterion in the tangential direction nearby the free boundary; thus, the radial cracks cross the rock sample from Zone 2 to the free surface (Zone 3). By comparing the results of simulation and experiment, it can be seen that the crack pattern induced by compression-shear, tension, and spalling is similar including the scales and the number of main cracks; the simulation result is in good agreement with the experimental crack pattern. Therefore, the currently developed numerical model

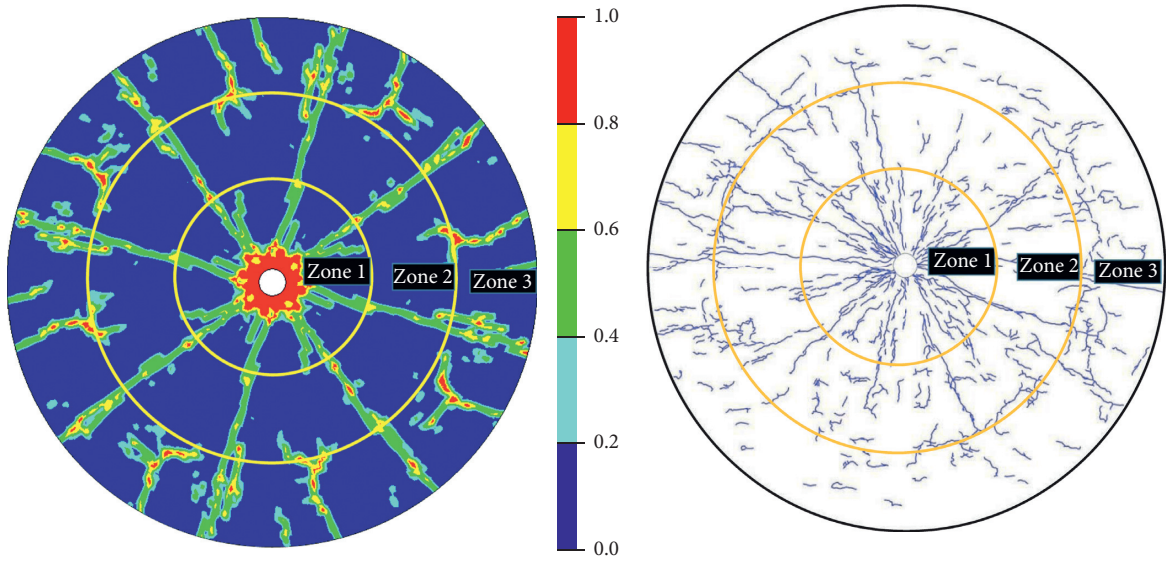

Figure 5: Comparison of (a) simulated crack pattern and (b) experimental crack pattern [58].

is applicable and suitable to simulate the crack evolution under blasting loading. In current simulation, the damage of the RHT material model is defined by using damage parameter $D = \sum \Delta\varepsilon^p/\varepsilon^f$, in which $\Delta\varepsilon^p$ is the accumulated plastic strain and ε^f is the failure strain. The damage of rock material (D) accumulates from 0 to 1, and different extents of rock damage can be denoted with different values of D from slight degradation to fully damaged. According to the comparison between the simulation result and experimental crack pattern, $D = 0.4$ and $D = 0.8$ denote that the crack is formed and the rock is crushed, respectively.

4. Numerical Simulation

As shown in Figure 6, in this study, a plane model of 6.0 m × 6.0 m with a centre hole ($x = y = 0$) of 100 mm diameter is built to investigate the rock crack propagation induced by blasting with a decoupled charge under high in situ stress. The number of elements is 1,440,000 with a mesh size of 5 mm × 5 mm × 5 mm. The elements at the interfaces between the parts of explosive, air, and rock mass share the common nodes. Nonreflecting boundaries are applied to the computational boundaries to model an infinite geologic body. For solving the problem of large deformation in rock blasting simulation, the multimaterial ALE method (ALE_MULTI-MATERIAL_GROUP) is adopted. Using this method, explosive and air materials are allowed to mix in each element in their corresponding meshes during calculation. There are two analysis phases for rock blasting under in situ stress. The first phase is for static analysis, and the second phase is for dynamic analysis. In the first phase, the in situ stress is applied to the boundaries of the model. The purpose is to obtain the stresses of each element induced by the initial pressure before blasting. In the second phase, a full restart operation is conducted, and the stresses of each element from the static analysis are input into the model as the

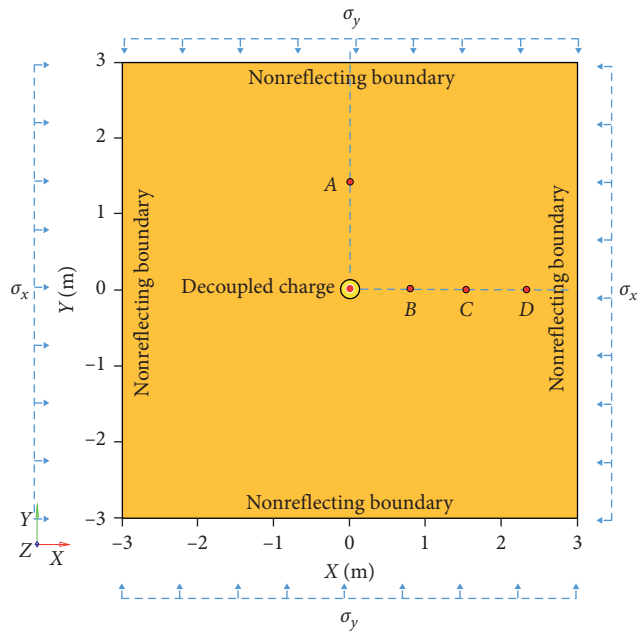

Figure 6: Layout of numerical model and boundary conditions.

initial stresses for the dynamic analysis. In order to analyze the mechanism of rock cracking under high in situ stress, four target points, i.e., A ($x = 0$, $y = 1.5$), B ($x = 0.75$, $y = 0$), C ($x = 1.5$, $y = 0$), and D ($x = 2.25$, $y = 0$), are selected to record the time-history data during calculation.

4.1. Consecutive Stages of Crack Propagation. Figures 7(a)–7(c) show the typical consecutive stages in the blast-induced rock cracking process under high in situ stress (the hydrostatic pressure is 30 MPa, and the decoupling coefficient is 1.25). When the explosive is detonated, a crushed zone (Zone I) is

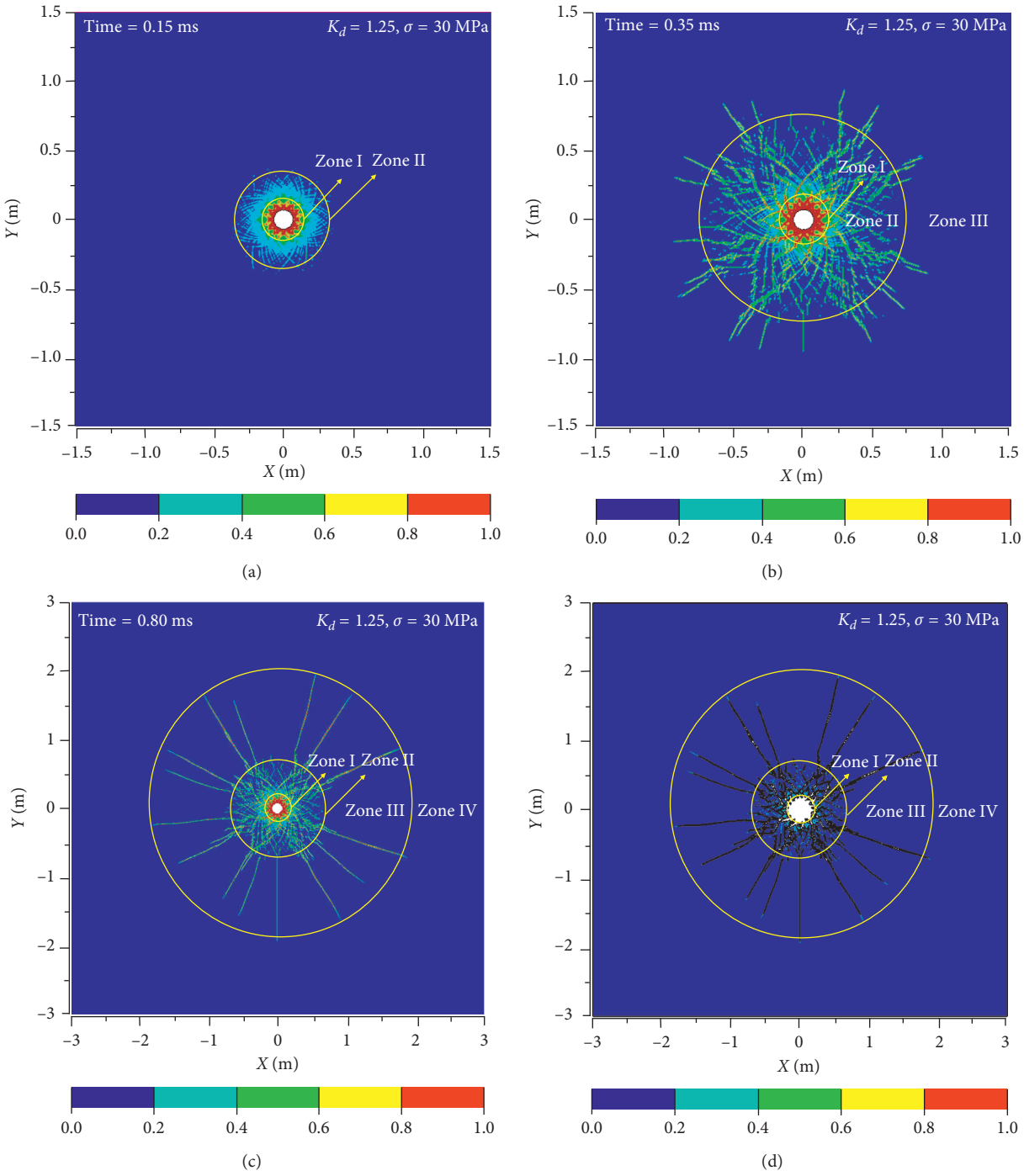

FIGURE 7: Consecutive stages of the blast-induced cracking process under high in situ stress ($K_d = 2.0$, $\sigma = 30$ MPa): (a) crushed zone; (b) crushed zone, nonlinear fracture zone, and radial crack propagation zone; (c) extension of the crushed zone, nonlinear fracture zone, and radial crack propagation zone; (d) crack pattern by blanking damaged elements.

immediately formed around the borehole since the strength of explosion shock waves greatly exceeds the dynamic compressive strength of the rock, and the rock is fully shattered. Thereafter, as the shock waves continue to propagate and dissipate in the second zone, i.e., the transitional and nonlinear zones or nonlinear fracture zone (Zone II), the particle size of fragmentation is rapidly increasing with radial distance, and the rock damage in this zone is range from severely crushed to partial fractured. Then, the crack propagates in the third zone, i.e., the elastic zone or the radial crack propagation zone (Zone III), where the cracking is predominately controlled by tensile stress component of blast-induced stress waves in the tangential direction around borehole. In this zone, the radial compressive stress is lower than the dynamic compressive strength of the rock, and therefore, it cannot cause crack

development. But since the tensile strength of the rock material is considerably smaller than the compressive strength, the tensile stress component is large enough to initiate radial cracks from the border of the nonlinear fracture zone and propagate in radial crack propagation zone. Compared to the inner two zones, the radial crack propagation zone is the largest one, and it is the most interesting damage zone regarding the breakage of rock. Eventually, when the tangential tensile stress component attenuates below the tensile strength of rock, the stress waves pass through the rock mass without further crack growth (Zone IV). Figure 7(d) shows the final crack pattern by blanking the damaged elements with the critical damage level $D = 0.4$ (crack forming).

4.2. Effect of In Situ Stress. Figure 8 shows the crack patterns of rock blasting under hydrostatic pressure 0, 10, 20, and 30 MPa with decoupling coefficient $K_d = 2.0$. As shown in Figure 8(a), when the blasting occurs without in situ stress, the radial cracks grow and some branches appear at the crack tips as they propagate away from the borehole. On the contrary, as shown in Figures 8(b)–8(d), the radial cracks propagate outward without noticeable branches at the crack tips when the rock mass is subjected to in situ stress. Furthermore, it can be seen from Figure 8 that the length of radial cracks rapidly decreases as the in situ stress increases. This is obviously because the in situ stress plays an important role in reducing tensile stress component in the tangential direction of borehole. As the propagation of crack mainly depends on the tensile stress component, the propagation of cracks is suppressed owing to the decline of tangential tensile stress. Besides the difference in the radial crack propagation zone, the rock cracking in the nonlinear fracture zone becomes severer (the number of cracks in the nonlinear fracture zone has a small increase with the increase in in situ stress). But since all of the increased cracks distribute in the vicinity of borehole, this phenomenon is not obvious. When the rock is subjected to continuously increased in situ stress, the shear fracture develops and gradually becomes the main damage pattern of rock mass. Thus, the increased number of rock cracks in the nonlinear fracture zone is mainly caused by the gradually aggravated shear damage as the confining pressure increases. Additionally, it can be found that the in situ stress has nearly no influence on the crushed zone. This is mainly because the explosion pressure is much higher than the initial static stress and the compressive strength of rock, and the rock crushing in the vicinity of the borehole is dominated by detonation pressure.

According to the above simulation results, when the rock blasting is conducted in deep mining, cracking in rock is suppressed by in situ stress; accordingly, the process of crack propagation induced by blasting is changed. Figure 9(a) shows the crack lengths with various in situ stresses. It can be seen that the crack length decreases gradually and the decrement of crack length in every MPa reduces as the in situ stress increases. This is because the tensile stress component decreases as the in situ stress increases. When the in situ stress is small, the length of radial crack is reduced rapidly with the increase in in situ stress. However, when the in situ stress is higher than 20 MPa, the radial crack is considerably short and it can only propagate in the vicinity of the nonlinear fracture zone. According to [3–7], the first two damage zones (the crushed zone and the nonlinear fracture zone) are mainly generated by compression-shear, and the last damage zone (the radial crack propagation zone) is induced by tension. With the increase in in situ stress, the area of the last damage zone decreases rapidly while the area of the first two damage zones does not change. Once the in situ stress is over 20 MPa, the area of the radial crack propagation zone is considerably small. In this situation, the compression-shear gradually becomes the main damage pattern of rock mass and the increase in in situ stress has no much influence on the crack evolution. As a result, the decrement of crack length decreases with the increase in in situ stress. Figure 9(b) shows the crack lengths at different times, the gradient (the gradient means to the velocity of crack propagation) of crack length vs time curves with low in situ stress is slightly higher than that of high in situ stress, and it can be concluded that the in situ stress has a small influence on reducing the velocity of crack propagation. Since the velocity of crack propagation decreases with the increase in in situ stress, the time of cracking at a certain point of rock mass is later with higher in situ stress. When the rock is subjected to high in situ stress, a small difference of damage time at a point, such as point A, can be observed. The higher the in situ stress is, the later the damage time will be. Additionally, it can also be found that higher in situ stress results in a shorter time of crack propagation. Once the strength of explosion stress wave is lower than the rock damage criterion, the crack propagation stops and no new crack generates.

Through comparison the results obtained from simulation and theoretical calculation, as shown in Figure 9(a), it can be seen that a similar tendency that the crack length decreases and the reduction of crack length in per MPa decrease with the increase in in situ stress, and it indicates that both the simulation and theoretical analysis provide good insights into the mechanism of blast-induced crack propagation when the rock is subjected to in situ stress. Nevertheless, there are still some differences between the simulation and theoretical results. The crack length obtained through theoretical calculation is slightly shorter than that of simulation under low in situ stress, while it is a little longer than the simulated value under high in situ stress. Meanwhile, as shown in Figure 9(b), the simulated velocity of crack propagation is higher than the theoretical value. This is mainly caused by the error accumulation during theoretical calculation on account of the simplified description of rock mass. Moreover, some influencing factors about rock blasting are not considered in this theoretical analysis such as strain hardening and damage softening. Therefore, it can be concluded that the theoretical analysis can be applied to predict the crack evolution, but due to the complexity of rock blasting under the influence of in situ stress, numerical simulation is a better way to precisely investigate the process of crack propagation.

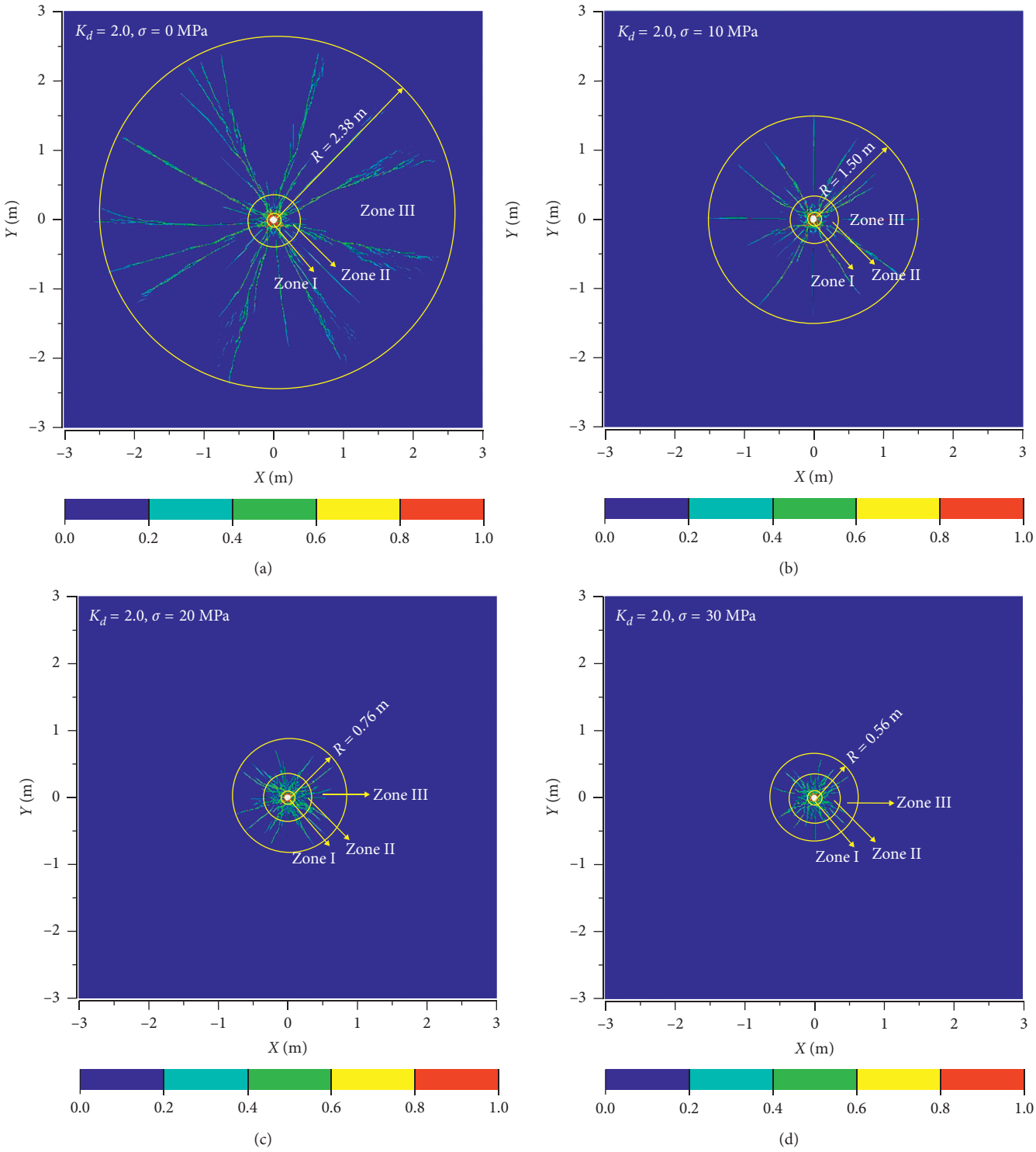

Figure 8: Crack patterns under different hydrostatic pressures (K_d = 2.0): (a) 0 MPa; (b) 10 MPa; (c) 20 MPa; (d) 30 MPa.

Figure 10 shows the radial stress-time curves at point C under in situ stresses of 0–50 MPa with an interval of 10 MPa. The negative value represents the compressive stress, and the positive value represents the tensile stress. As can be seen from the picture, the stress-time curve with a lower in situ stress is below that of the higher one at the loading and unloading stages. The corresponding peak radial compressive stresses (at 0.31 ms) are −119.2, −129.9, −140.2, −152.3, −162.8, and −174.6 MPa for in situ stress at 0, 10, 20, 30, 40, and 50 MPa, respectively. This implies that the peak stress directly relates to the magnitude of in situ stress, and a higher in situ stress leads to a larger peak compressive stress. At the same time, with the increase in in situ stress, the radial stress of tensile (at 0.34 ms) has a descending tendency. The

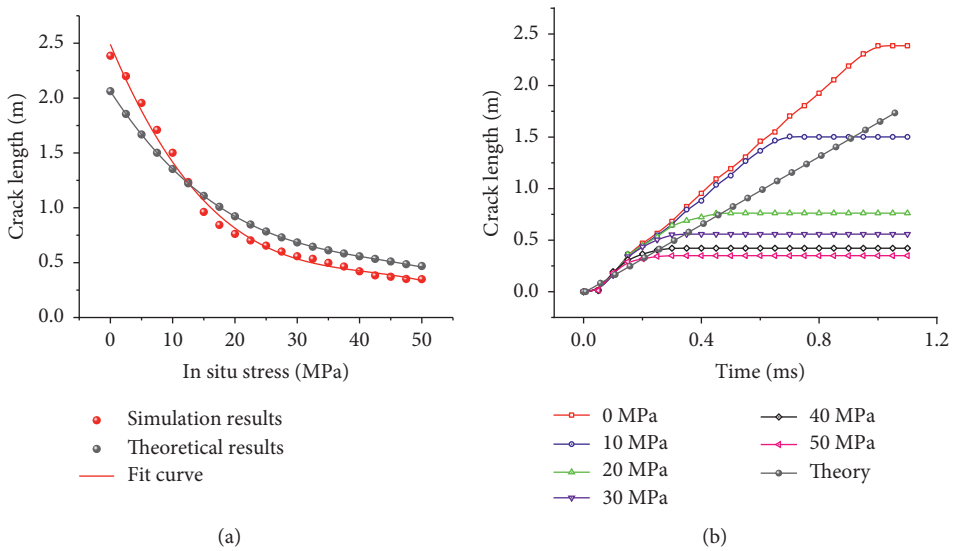

Figure 9: Crack lengths (a) with various in situ stresses (b) at different times ($K_d = 2.0$).

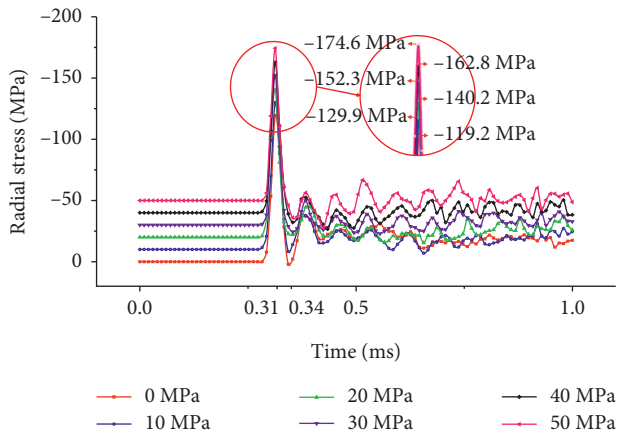

Figure 10: Time-history curves of radial stress at point C under different hydrostatic pressures.

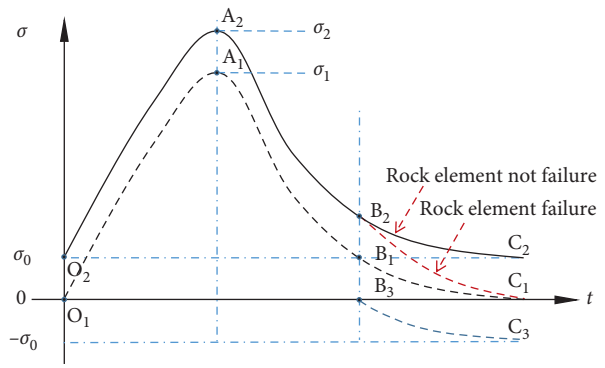

Figure 11: Loading and unloading curves under the combination of in situ stress and blast loading.

corresponding maximum tensile stress in the radial direction is 2.14 MPa for in situ stress 0 MPa, and it converts into compressive stress with the in situ stress increasing. Thus, it can be drawn that the in situ stress is mainly responsible for increasing compressive stress and decreasing tensile stress component in the radial direction of borehole under blast loading.

Through the above analysis based on the time-history curves of radial stress at point C, the loading and unloading mechanisms of rock blasting with in situ stress and without in situ stress can be explained in Figure 11. $O_1A_1B_1C_1$ is the original loading and unloading curve without in situ stress, and the horizontal line O_2B_2 represents in situ stress σ_0. In the loading stage, when the in situ stress is 0 MPa, the explosion stress waves are immediately exerted on the rock mass in the radial direction after the explosive is detonated, and the peak stress is σ_1. On the contrary, when the in situ stress is σ_0, the peak stress reaches $\sigma_2 = \sigma_1 + \sigma_0$. In the unloading stage, two cases may occur based upon whether the rock element is damaged during blast loading. Case 1: the rock element is not damaged during rock blasting, and the stress in rock element is unloading from the peak stress to the initial stress level. The unloading curves can be denoted by $A_1B_1C_1$ and $A_2B_2C_2$ when the in situ stress is 0 MPa and σ_0, respectively. Case 2: the rock element is damaged under blast loading, and the stress in rock mass is unloading from the peak stress to 0 MPa. The unloading curve under in situ stress condition changes to $A_2B_2C_1$. When the stress decays to σ_0, the transient release of in situ stress occurs. B_3C_3 denotes the unloading curve of in situ stress, and B_2C_1 is a curve superposed by B_2C_2 and B_3C_3.

Figure 12 shows the peak pressures and peak particle velocities (PPVs) under different in situ stresses at points B, C, and D. It can be seen that both the peak pressure and PPV increase with the increase in in situ stress. As we all know, when the deep-buried rock is fragmented by blasting, the high in situ stress resists the rock damage. This means as the in situ stress increases, the explosion energy consumed in rock fragmentation presents a

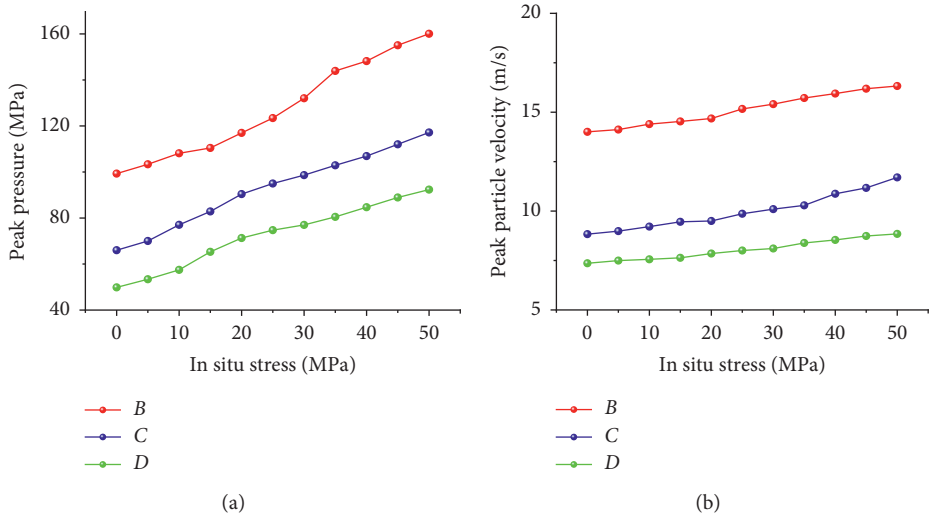

Figure 12: (a) Peak pressures and (b) peak particle velocities (PPVs) under different in situ stresses at points *B*, *C*, and *D*.

declining trend and more explosion energy is consumed in rock vibration. In this situation, the increase in peak pressure is caused by the superposition of explosion stress waves and initial static stress, and the increase in PPV is induced by stress waves passing through the rock mass without rock damage. Thus, it can be concluded that the in situ stress plays an important role in increasing the peak pressure and PPV in rock mass subjected to in situ stress and blast loading.

4.3. Effect of Lateral Pressure Coefficient. In deep rock blasting, the in situ stress field around the cross section of borehole is usually biaxial [38], and the orthotropic in situ stresses may cause stress concentration in the vicinity of the borehole and further leads to the asymmetrical crack pattern. In order to investigate the crack propagation resulted by blasting in the biaxial stress field, preload of 50 MPa is imposed on the model in the *X*-direction and preloads of 10, 20, 30, and 40 MPa are applied on the model in the *Y*-direction, respectively. By this, the separate lateral pressure coefficients are 1.25, 1.67, 2.5, and 5. Figure 13 shows the crack patterns under different biaxial stresses. It can be seen that the cracks are obviously aligned with the direction of maximum principal stress. Moreover, the anisotropy of the cracks becomes more and more distinct as the difference between two principal stresses increases. This is obviously because the tensile stress component perpendicular to the crack propagation direction is suppressed by the preloaded pressure. When the preloaded pressure in the *X*-direction is higher than that in the *Y*-direction, the tensile stress component in the *X*-direction is suppressed severely. As a result, the crack preferentially grows in the *X*-direction, i.e., the direction of maximum principal stress. This is the reason why difficulties are always encountered in presplitting or smooth blasting of underground opening, which is subjected to biaxial in situ stresses.

Figure 14 gives a comparison of the crack lengths in the *X*-direction under hydrostatic pressure ($\sigma_x = \sigma_y = 10$, 20, 30, and 40 MPa) and nonhydrostatic pressure ($\sigma_x = 50$ MPa; $\sigma_y = 10$, 20, 30, and 40 MPa) conditions. Under the condition of nonhydrostatic pressure, the *X*-direction pressure is kept 50 MPa and the *Y*-direction pressure is changed from 10 MPa to 40 MPa. It can be seen that when the *X*-directional stress is identical, the crack lengths are similar and there is almost no difference between the situations of hydrostatic and nonhydrostatic pressures. This indicates that the crack length is not affected by the in situ stress, which is parallel to the direction of crack propagation. On the contrary, as shown in Figure 13, the crack length in the *X*-direction decreases as the second principal stress increases in the *Y*-direction. Therefore, it can be concluded that the crack length is mainly controlled by the preloaded pressure vertical to the direction of crack propagation.

Since the crack length of rock blasting is predominantly controlled by the preloaded stress vertical to the direction of crack propagation, the stress-time curves in the *Y*-direction (the direction vertical to the main cracks as shown in Figure 13) are examined. Figure 15 shows the comparison of the radial stress-time curves at point *A* under the situations of hydrostatic pressure and nonhydrostatic pressure, and the in situ stresses in the *Y*-direction are 10, 20, 30, and 40 MPa, respectively. Differing from the hydrostatic pressure field, the in situ stress keeps 50 MPa in the *X*-direction under every nonhydrostatic pressure situation. It can be seen that the stress-time curves are consistent between the situations of hydrostatic pressure and nonhydrostatic pressure when the initial stresses in the *Y*-direction are same, and the *Y*-directional stress increases with the increase in applied stress in the *Y*-direction. Based on these, two conclusions can be obtained; firstly, the *Y*-directional stress-time curves are not affected by the applied stress in the *X* direction; secondly, the curve of radial stress in the *Y*-direction is only controlled by the applied pressure in the *Y*-direction. Therefore, it can be

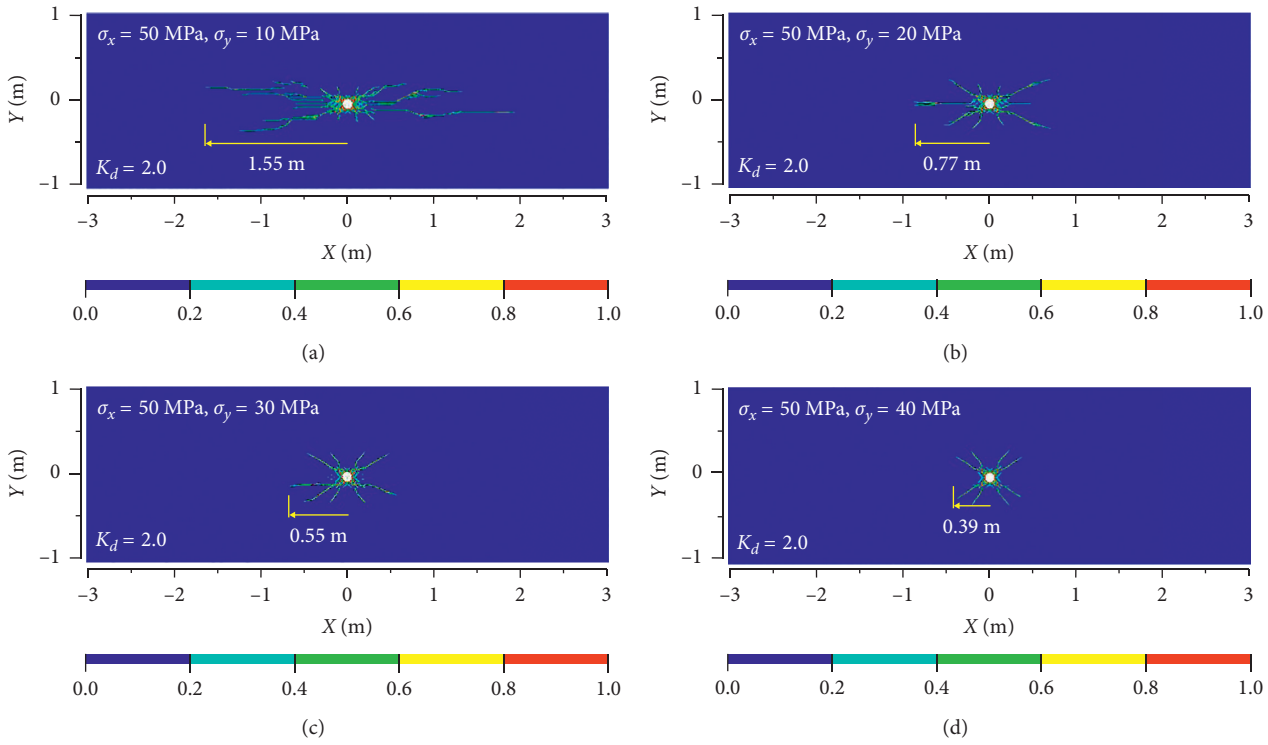

Figure 13: Crack patterns in different biaxial stress fields ($K_d = 2.0$): (a) $\sigma_x = 50$ MPa and $\sigma_y = 10$ MPa; (b) $\sigma_x = 50$ MPa and $\sigma_y = 20$ MPa; (c) $\sigma_x = 50$ MPa and $\sigma_y = 30$ MPa; (d) $\sigma_x = 50$ MPa and $\sigma_y = 40$ MPa.

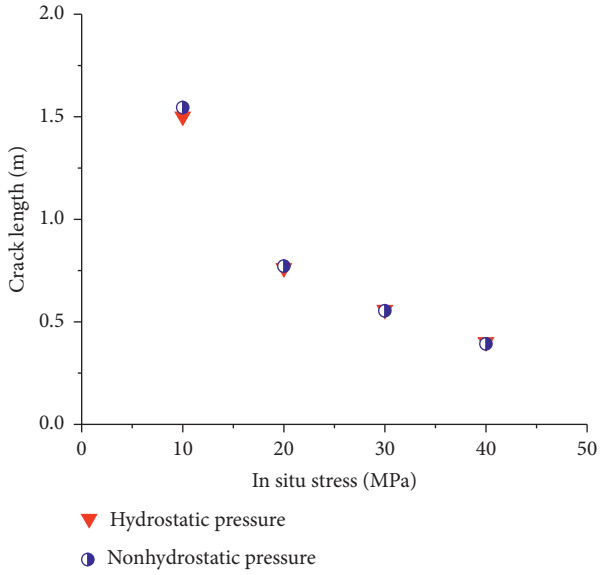

Figure 14: Comparison of crack lengths between the situations of hydrostatic pressure and nonhydrostatic pressure ($\sigma_x = 50$ MPa) in the X-direction.

drawn that the in situ stress is mainly responsible for changing the stress-time curves aligning the direction of the applied pressure, and the loading and unloading curves in biaxial directions are separately controlled by two orthotropic stresses.

4.4. Effect of Decoupling Coefficient. Since the high in situ stress greatly suppresses the propagation of the radial crack, for an expected fragmentation of rock mass, the amount of explosive in borehole should be increased accordingly. Figure 16 shows the crack patterns with various charge

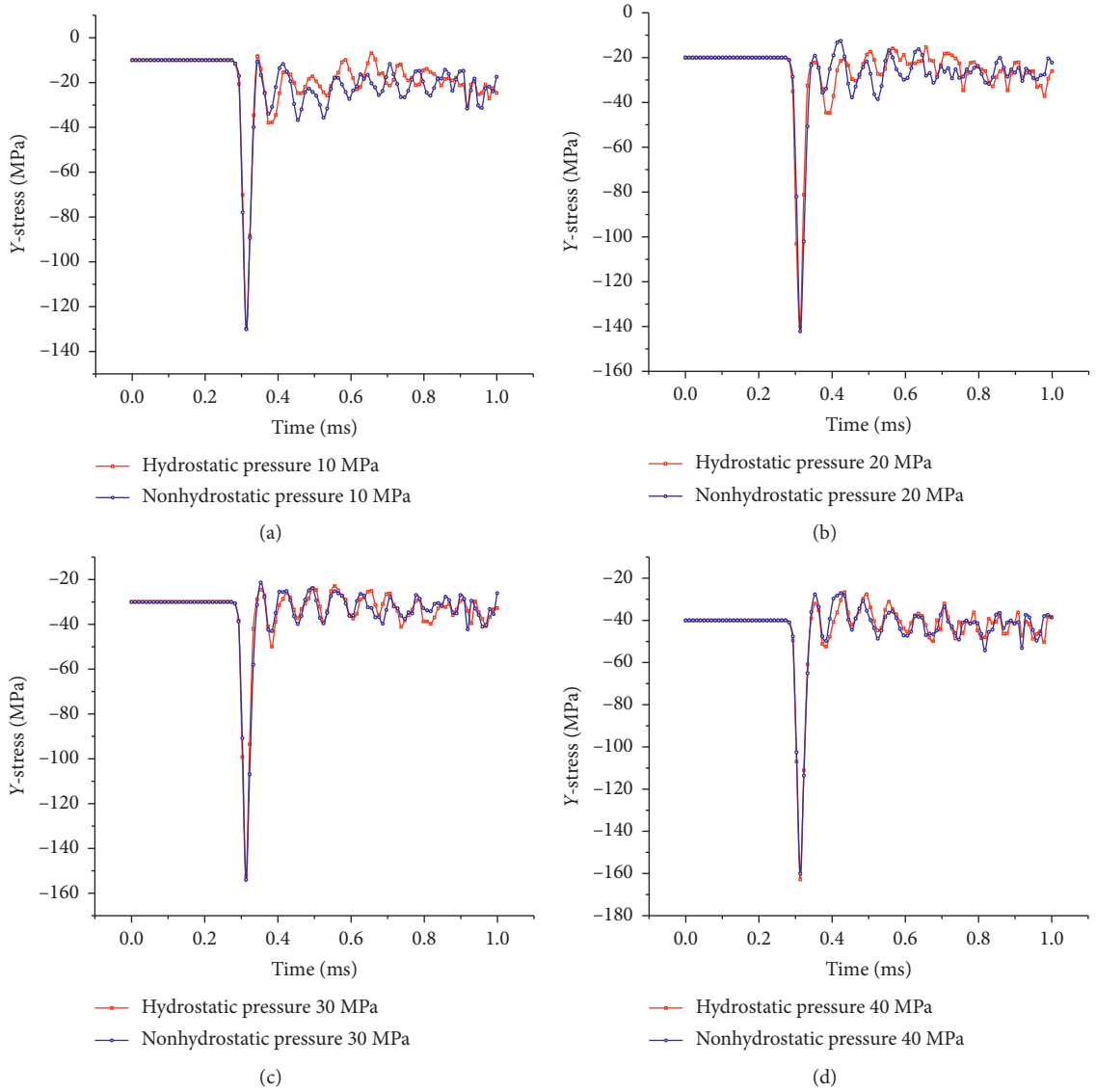

FIGURE 15: Comparisons of the Y-stress time-history curves at point A between the situations of hydrostatic pressure ($\sigma_x = \sigma_y$, $K_d = 2.0$) and nonhydrostatic pressure ($\sigma_x = 50$ MPa, $K_d = 2.0$): (a) $\sigma_y = 10$ MPa; (b) $\sigma_y = 20$ MPa; (c) $\sigma_y = 30$ MPa; (d) $\sigma_y = 40$ MPa.

diameters under hydrostatic pressure 30 MPa, and the decoupling coefficients K_d are 1.67, 1.43, 1.25, and 1.11, respectively. As can be seen from the pictures, all the areas of crushed zones, nonlinear fracture zones, and radial crack propagation zones increase with the decrease in decoupling coefficient. As expected, the more the explosive is, the more the rock mass is fractured by blasting.

Figure 17 shows the crack lengths with different decoupling coefficients under in situ stress 0, 10, 20, 30, 40, and 50 MPa, respectively. It can be seen that, after a slower rise stage in the curve of crack length, a rapidly increasing stage can be observed in all the curves as $1/K_d$ increases, and then a slower rise stage in the curve of crack length is encountered again. This is because there is a biggest decoupling coefficient (the smallest amount of explosive) existed for the crack initiation when the rock mass is under the in situ stress condition, and the rock cracking is obviously intensified as the charge diameter increases. In the first slower rise stage and the rapidly increasing stage of Figure 17, the rock fragmentation is mostly controlled by radial cracks induced by tensile stress component. But once the decoupling coefficient decreases to a critical value, the main damage pattern of rock mass converts to crush by compression and shear. A great part of explosion energy is consumed for smashing the rock mass, and the pulverized rock works as a filter to reduce the energy transmission from the explosion products to outer rock mass. In the second slower rise stage of Figure 17, a small part of explosion energy will be consumed on the evolution of radial cracks. Consequently, an optimal decoupling coefficient exists under in situ stress situation, and when the optimal decoupling coefficient is employed, the utilization efficiency of explosive energy in rock fragmentation can be maximized.

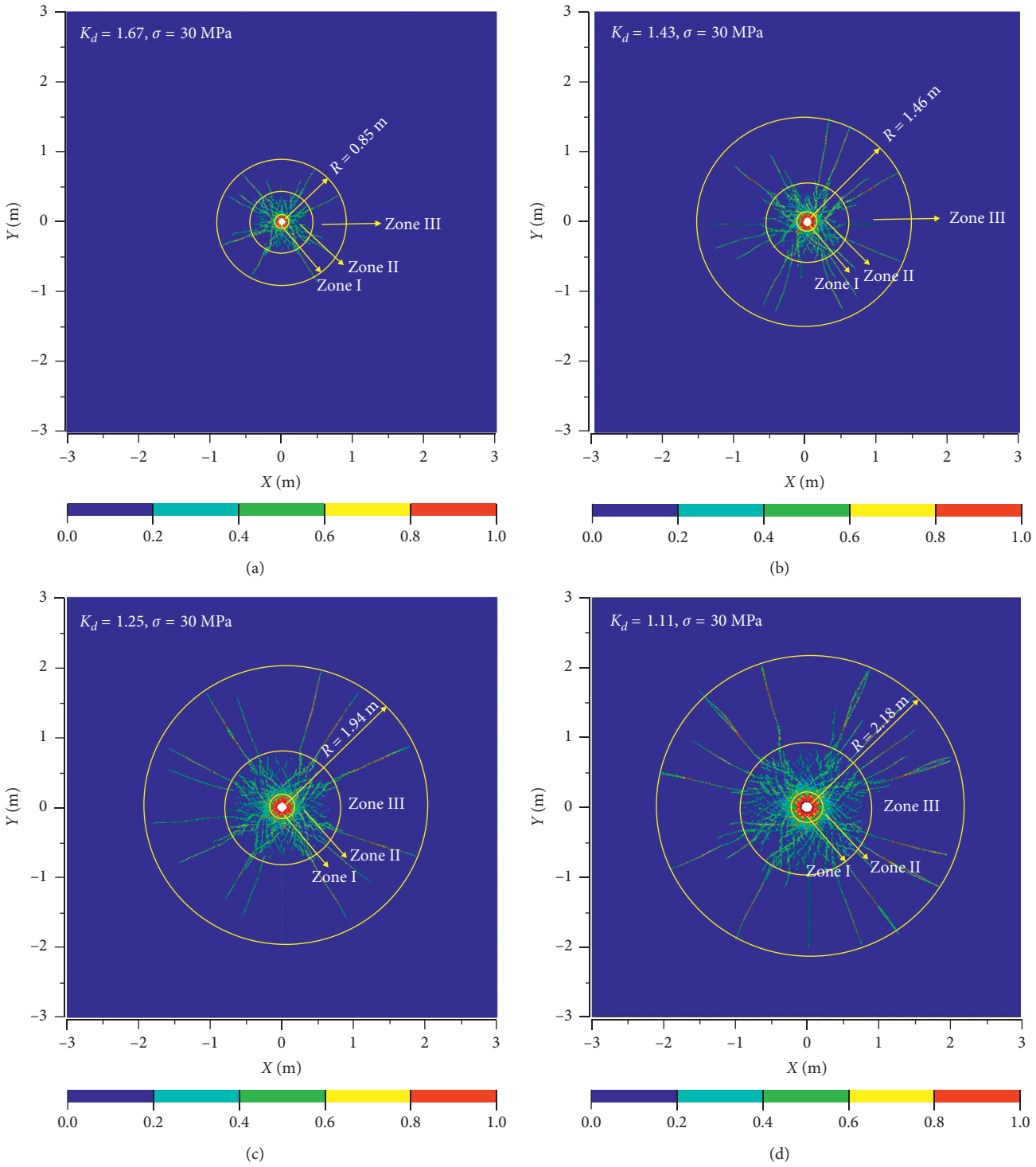

FIGURE 16: Crack patterns with different decoupling coefficients under hydrostatic pressure 30 MPa: (a) $K_d = 1.67$; (b) $K_d = 1.43$; (c) $K_d = 1.25$; (d) $K_d = 1.11$.

For efficiently fragmenting rock mass in deep rock blasting, parameter D_A is defined as $D_A = A_c/m_e$ to evaluate the utilization efficiency of explosive energy, where A_c is the area of rock fragmentation and m_e is the amount of explosive. Figure 18 shows the curves of D_A with various charge diameters under different in situ stresses, and it shown that the higher the in situ stress is, the lower the utilization efficiency of explosive energy will be. Furthermore, peak values in the curves of D_A can be observed. According to the simulation results, the optimal decoupling coefficients are 2.65, 1.87, 1.37, and 1.22 for 0, 10, 20, and 30 MPa, respectively, and the optimal decoupling coefficient

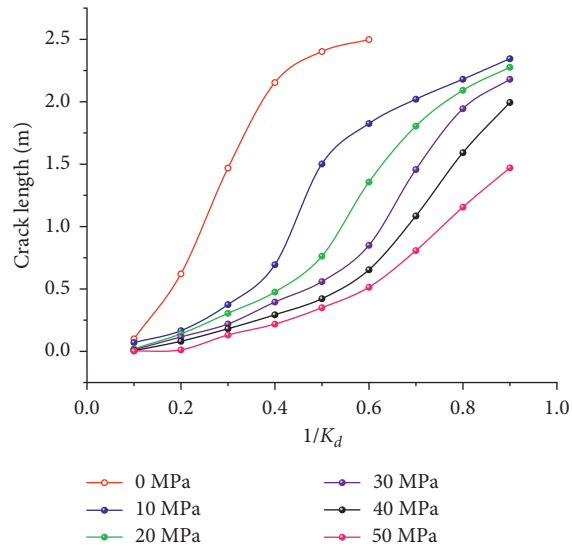

Figure 17: Crack lengths with different decoupling coefficients and different in situ stresses.

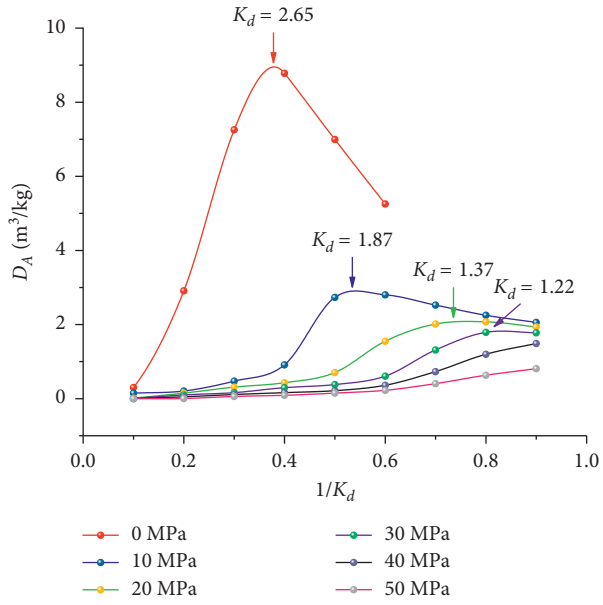

Figure 18: D_A curves under different in situ stresses.

reduces with the increase in in situ stress. In addition, when the in situ stress is higher than 30 MPa, the optimal decoupling coefficient is smaller than 1.22, which means that more explosive should be provided.

5. Conclusions

In this paper, the blast-induced crack propagation with a decoupled charge under in situ stress is first analyzed by a theoretical approach, and then a numerical model is built to reveal how the in situ stress and the decoupled charge affect the rock crack initiation and propagation during blasting. According to the simulation, the mechanisms of loading and unloading, as well as the process of rock cracking under different situations of hydrostatic pressure and non-hydrostatic pressure, are investigated. The differences in rock cracking with different decoupling coefficients subjected to high in situ stress are also examined. This study provides a reference to address excavation difficulties related to deep mining. Based on the analyses above, the following conclusions can be drawn:

(1) When the rock blasting is conducted with a decoupled charge under high in situ stress, three damage zones, i.e., the crushed zone, the nonlinear fracture zone, and the radial crack propagation zone, are formed.

(2) The crack formation is greatly suppressed by high in situ stress in the radial crack propagation zone. However, the high in situ stress has no much influence on crack evolution in the crushed zone and the nonlinear fracture zone. The velocity of crack propagation is reduced, and the process of crack propagation is stopped in advance when the rock mass is subjected to high in situ stress. Additionally, the in situ stress plays an important role in increasing the peak pressure and PPV in rock mass which is subjected to high in situ stress and blasting loading.

(3) The radial crack is aligned with the direction of maximum principal stress, and the radial crack propagation is mainly controlled by the preloaded stress vertical to the direction of crack propagation. The anisotropy of crack propagation becomes more obvious when the difference between the applied biaxial stresses increases, and it may cause pre-splitting or smooth blasting difficulties in deep rock engineering which is subjected to biaxial stresses.

(4) The optimal decoupling coefficients exist under different in situ stresses, and the optimal decoupling coefficients reduce with the increase in in situ stress; the corresponding optimal decoupling coefficients are 2.65, 1.87, 1.37, and 1.22 for 0, 10, 20, and 30 MPa, respectively.

Data Availability

The data used to support the findings of this study are available from the corresponding author upon request.

Conflicts of Interest

The authors declare that there are no conflicts of interest regarding the publication of this paper.

Acknowledgments

The authors acknowledge the financial support from the National Science Foundation of China under Grant no. 51974360, Natural Science Foundation of Hunan Province, China, under grant no. 2018JJ3656, Fundamental Research Funds for Central Universities of Central South University under grant no. 1053320183209, and National Key Research

and the Development Program of China under Grant no. 2016YFC0600802 for carrying out this research work.

References

[1] C. Fairhurst, "Some challenges of deep mining," *Engineering*, vol. 3, no. 4, pp. 527–537, 2017.

[2] A. M. Lucier, M. D. Zoback, V. Heesakkers, Z. E. Reches, and S. K. Murphy, "Constraining the far-field in situ stress state near a deep South African gold mine," *International Journal of Rock Mechanics and Mining Sciences*, vol. 46, no. 3, pp. 555–567, 2009.

[3] H. M. An, H. Y. Liu, H. Han, X. Zheng, and X. G. Wang, "Hybrid finite-discrete element modelling of dynamic fracture and resultant fragment casting and muck-piling by rock blast," *Computers and Geotechnics*, vol. 81, pp. 322–345, 2017.

[4] C. P. Yi, D. Johansson, and J. Greberg, "Effects of in-situ stresses on the fracturing of rock by blasting," *Computers and Geotechnics*, vol. 104, pp. 321–330, 2017.

[5] L. X. Xie, W. B. Lu, Q. B. Zhang, Q. H. Jiang, G. H. Wang, and J. Zhao, "Damage evolution mechanisms of rock in deep tunnels induced by cut blasting," *Tunnelling and Underground Space Technology*, vol. 58, pp. 257–270, 2016.

[6] L. X. Xie, W. B. Lu, Q. B. Zhang, Q. H. Jiang, M. Chen, and J. Zhao, "Analysis of damage mechanisms and optimization of cut blasting design under high in-situ stresses," *Tunnelling and Underground Space Technology*, vol. 66, pp. 19–33, 2017.

[7] H. K. Kutter and C. Fairhurst, "On the fracture process in blasting," *International Journal of Rock Mechanics and Mining Sciences and Geomechanics Abstracts*, vol. 8, no. 3, 1971.

[8] H. P. Rossmanith, R. E. Knasmillner, A. Daehnke, and L. Mishnaevsky, "Wave propagation, damage evolution, and dynamic fracture extension," *Materials Science*, vol. 32, no. 4, 1996.

[9] L. Y. Yang, R. S. Yang, and P. Xu, "Experimental study on the effect of initial compression stress field on blast-induced crack behaviors," *Journal of China Coal Society*, vol. 38, no. 3, pp. 404–410, 2013, in Chinese.

[10] L. Y. Yang and C.-X. Ding, "Fracture mechanism due to blast-imposed loading under high static stress conditions," *International Journal of Rock Mechanics and Mining Sciences*, vol. 107, pp. 150–158, 2018.

[11] R. H. Nilson, W. J. Proffer, and R. E. Duff, "Modelling of gas-driven fractures induced by propellant combustion within a borehole," *International Journal of Rock Mechanics and Mining Sciences & Geomechanics Abstracts*, vol. 22, no. 1, pp. 3–19, 1985.

[12] N. R. Warpinski, R. A. Schmidt, and P. W. Cooper, "High-energy gas frac: multiple fracturing in a Wellbore," in *Proceedings of the 20th US Symposium on Rock Mechanics (USRMS)*, Austin, TX, USA, June 1979.

[13] R. A. Schmidt, N. R. Warpinski, and P. W. Cooper, *In Situ Evaluation of Several Tailored-Pulse Well-Shooting Concepts*, Sandia National Labs., Albuquerque, NM, USA, 1980.

[14] J. F. Cuderman, *Multiple Fracturing Experiments: Propellant and Borehole Considerations*, Sandia National Labs., Albuquerque, NM, USA, 1982.

[15] A. S. Paine and C. P. Please, "An improved model of fracture propagation by gas during rock blasting-some analytical results," *International Journal of Rock Mechanics and Mining Sciences & Geomechanics Abstracts*, vol. 31, no. 6, pp. 699–706, 1994.

[16] W. B. Lu and Z. Y. Tao, "A study of fracture propagation velocity driven by gases of explosion products," *Explosion and Shock Waves*, vol. 14, no. 3, pp. 264–268, 1994, in Chinese.

[17] W. Lu, M. Chen, X. Geng, D. Shu, and C. Zhou, "A study of excavation sequence and contour blasting method for underground powerhouses of hydropower stations," *Tunnelling and Underground Space Technology*, vol. 29, pp. 31–39, 2012.

[18] Y. G. Hu, W. B. Lu, X. X. Wu, M. Liu, and P. Li, "Numerical and experimental investigation of blasting damage control of a high rock slope in a deep valley," *Engineering Geology*, vol. 237, pp. 12–20, 2018.

[19] Z. Zhu, "Numerical prediction of crater blasting and bench blasting," *International Journal of Rock Mechanics and Mining Sciences*, vol. 46, no. 6, pp. 1088–1096, 2009.

[20] J. P. Latham, A. Munjiza, and P. Lu, "Rock fragmentation by blasting-a literature study of research in the 1980's and 1990's," *Fragblast*, vol. 3, no. 3, pp. 193–212, 1999.

[21] M. R. Saharan, H. S. Mitri, and J. L. Jethwa, "Rock fracturing by explosive energy: review of state-of-the-art," *Fragblast*, vol. 10, no. 1-2, pp. 61–81, 2006.

[22] D. S. Preece and B. J. Thorne, "A study of detonation timing and fragmentation using 3D finite element techniques and damage constitutive model," *Fragblast*, vol. 5, pp. 147–156, 1996.

[23] M. Bendezu, C. Romanel, and D. Roehl, "Finite element analysis of blast-induced fracture propagation in hard rocks," *Computers & Structures*, vol. 182, pp. 1–13, 2017.

[24] E. Rougier, C. R. Bradley, and S. T. Broom, *The Combined Finite-Discrete Element Method Applied to the Study of Rock Fracturing Behavior in 3D*, Los Alamos National Lab.(LANL), Los Alamos, NM, USA, 2011.

[25] A. A. Munjiza, E. E. Knight, and E. Rougier, *Computational Mechanics of Discontinua*, John Wiley & Sons, Hoboken, NJ, USA, 2011.

[26] A. A. Munjiza, *The Combined Finite-Discrete Element Method*, John Wiley & Sons, Hoboken, NJ, USA, 2004.

[27] A. A. Munjiza, E. E. Knight, and E. Rougier, *Large Strain Finite Element Method: A Practical Course*, John Wiley & Sons, Hoboken, NJ, USA, 2015.

[28] J. P. Latham, A. Munjiza, X. Garcia, J. Xiang, and R. Guises, "Three-dimensional particle shape acquisition and use of shape library for DEM and FEM/DEM simulation," *Minerals Engineering*, vol. 21, no. 11, pp. 797–805, 2008.

[29] Z. Lei, E. Rougier, E. E. Knight, A. Munjiza, and H. Viswanathan, "A generalized anisotropic deformation formulation for geomaterials," *Computational Particle Mechanics*, vol. 3, no. 2, pp. 215–228, 2016.

[30] Z. Lei, E. Rougier, A. Munjiza, H. Viswanathan, and E. E. Knight, "Simulation of discrete cracks driven by nearly incompressible fluid via 2D combined finite-discrete element method," *International Journal for Numerical and Analytical Methods in Geomechanics*, vol. 43, no. 9, pp. 1724–1743, 2019.

[31] A. Munjiza, V. Divic, and B. Mohanty, "Frontiers and challenges in numerical simulation of the blasting process using the combined finite discrete element method," *Rock Fragmentation by Blasting*, vol. 10, pp. 15–21, 2013.

[32] J. P. Latham, P. Yang, and Q. Lei, "Blast fragmentation in rock with discontinuities using an equation of state gas model coupled to a transient dynamics fracturing and fragmenting FEMDEM model," in *Proceedings of the 51st US Rock Mechanics/Geomechanics Symposium*, American Rock Mechanics Association, San Francisco, CA, USA, June 2017.

[33] D. S. Preece and S. H. Chung, "An algorithm for improving 2-D and 3-D spherical element behavior during formation of

muck piles resulting from rock blasting," in *Proceedings of the Discrete Element Methods: Numerical Modeling of Discontinua*, pp. 62–67, Santa Fe, NM, USA, September 2002.

[34] D. Owen, A. Munjiza, and N. Bicanic, "A finite element-discrete element approach to the simulation of rock blasting problems," in *Proceedings of the 11th Symposium on Finite Element Methods*, Cape Town, South Africa, September 1992.

[35] J. P. Latham, Q. Lei, and A. Obeysekara, "Recent advances in hydromechanical modelling of fractured rocks using the finite-discrete element method," in *Proceedings of the International Conference on Coupled Processes in Fractured Geological Media*, Wuhan, China, November 2018.

[36] A. Lisjak and G. Grasselli, "A review of discrete modeling techniques for fracturing processes in discontinuous rock masses," *Journal of Rock Mechanics and Geotechnical Engineering*, vol. 6, no. 4, pp. 301–314, 2014.

[37] W. Lu, J. Yang, P. Yan et al., "Dynamic response of rock mass induced by the transient release of in-situ stress," *International Journal of Rock Mechanics and Mining Sciences*, vol. 53, pp. 129–141, 2012.

[38] G. W. Ma and X. M. An, "Numerical simulation of blasting-induced rock fractures," *International Journal of Rock Mechanics and Mining Sciences*, vol. 45, no. 6, pp. 966–975, 2008.

[39] J. H. An, C. Yao, Q. H. Jiang, W. B. Lu, and S. H. Jiang, "2D numerical analysis of rock damage induced by dynamic in-situ stress redistribution and blast loading in underground blasting excavation," *Tunnelling and Underground Space Technology*, vol. 70, pp. 221–232, 2017.

[40] O. Yilmaz and T. Unlu, "Three dimensional numerical rock damage analysis under blasting load," *Tunnelling and Underground Space Technology*, vol. 38, pp. 266–278, 2013.

[41] F. V. Donzé, J. Bouchez, and S. A. Magnier, "Modeling fractures in rock blasting," *International Journal of Rock Mechanics and Mining Sciences*, vol. 34, no. 8, pp. 1153–1163, 1997.

[42] K. Liu, H. Hao, and X. Li, "Numerical analysis of the stability of abandoned cavities in bench blasting," *International Journal of Rock Mechanics and Mining Sciences*, vol. 92, pp. 30–39, 2017.

[43] Z. L. Zhou, R. S. Cheng, X. Cai, D. Ma, and C. Jiang, "Discrimination of rock fracture and blast events based on signal complexity and machine learning," *Shock and Vibration*, vol. 2018, Article ID 9753028, 10 pages, 2018.

[44] Z. L. Zhou, R. S. Cheng, X. Cai, J. Jia, and W. Wang, "Comparison of presplit and smooth blasting methods for excavation of rock wells," *Shock and Vibration*, vol. 2019, Article ID 3743028, 12 pages, 2019.

[45] S. McHugh, "Crack extension caused by internal gas pressure compared with extension caused by tensile stress," *International Journal of Fracture*, vol. 21, no. 3, pp. 163–176, 1983.

[46] P. A. Persson, N. Lundborg, and C. H. Johansson, "The basic mechanisms in rock blasting," *International Society of Rock Mechanics Proceedings*, vol. 3, pp. 19–33, 1970.

[47] H. E. Erhie, *Mathematical Aspects of the Modelling of Rock Blasting*, University of Southampton, Southampton, UK, 1990.

[48] J. Henrych and R. Major, *The Dynamics of Explosion and its Use*, Academia Prague, Prague, Czech Republic, 1979.

[49] G. I. Barenblatt, "The mathematical theory of equilibrium cracks in brittle fracture," *Advances in Applied Mechanics*, vol. 7, pp. 55–129, 1962.

[50] Z. X. Zhang, S. Q. Kou, L. G. Jiang, and P.-A. Lindqvist, "Effects of loading rate on rock fracture: fracture characteristics and energy partitioning," *International Journal of Rock Mechanics and Mining Sciences*, vol. 37, no. 5, pp. 745–762, 2000.

[51] T. Yin, L. Bai, X. Li, X. Li, and S. Zhang, "Effect of thermal treatment on the mode I fracture toughness of granite under dynamic and static coupling load," *Engineering Fracture Mechanics*, vol. 199, pp. 143–158, 2018.

[52] Z. Yin, W. Chen, H. Hao et al., "Dynamic compressive test of gas-containing coal using a modified split hopkinson pressure bar system," *Rock Mechanics and Rock Engineering*, vol. 53, no. 2, pp. 815–829, 2019.

[53] D. Ma, J. Wang, X. Cai et al., "Effects of height/diameter ratio on failure and damage properties of granite under coupled bending and splitting deformation," *Engineering Fracture Mechanics*, vol. 220, Article ID 106640, 2019.

[54] D. Ma, H. Duan, X. Li, Z. Li, Z. Zhou, and T. Li, "Effects of seepage-induced erosion on nonlinear hydraulic properties of broken red sandstones," *Tunnelling and Underground Space Technology*, vol. 91, Article ID 102993, 2019.

[55] S. Q. Peng, F. Wang, X. B. Li, L. Fan, and F. Gong, "A microbial method for improving salt swelling behavior of sulfate saline soil by an experimental study," *Alexandria Engineering Journal*, vol. 58, no. 4, pp. 1353–1366, 2019.

[56] M. J. Iqbal and B. Mohanty, "Experimental calibration of isrm suggested fracture toughness measurement techniques in selected brittle rocks," *Rock Mechanics and Rock Engineering*, vol. 40, no. 5, pp. 453–475, 2007.

[57] B. Lawn and T. R. Wilshaw, *Fracture of Brittle Solids*, Cambridge University Press, Cambridge, UK, 1993.

[58] M. M. D. Banadaki, *Stress-wave Induced Fracture in Rock Due to Explosive Action*, University of Toronto, Scarborough, Canada, 2010.

[59] M. M. D. Banadaki and B. Mohanty, "Numerical simulation of stress wave induced fractures in rock," *International Journal of Impact Engineering*, vol. 40-41, pp. 16–25, 2012.

[60] W. Riedel, N. Kawai, and K.-I. Kondo, "Numerical assessment for impact strength measurements in concrete materials," *International Journal of Impact Engineering*, vol. 36, no. 2, pp. 283–293, 2009.

[61] W. Riedel, K. Thoma, and S. Hiermaier, "Penetration of reinforced concrete by BETA-B-500 numerical analysis using a new macroscopic concrete model for hydrocodes," in *Proceedings of the 9th International Symposium on the Effects of Munitions with Structures*, vol. 315, Berlin, Germany, May 1999.

[62] T. Borrvall and W. Riedel, "The RHT concrete model in LS-DYNA," in *Proceedings of the 8th European LS-DYNA User Conference*, Strasbourg, France, May 2011.

[63] E. L. Lee, H. C. Hornig, and J. W. Kury, *Adiabatic Expansion of High Explosive Detonation Products*, University of California Radiation Lab, Livermore, CA, USA, 1968.

[64] X. Y. Wei, Z. Y. Zhao, and J. Gu, "Numerical simulations of rock mass damage induced by underground explosion," *International Journal of Rock Mechanics and Mining Sciences*, vol. 46, no. 7, pp. 1206–1213, 2009.

[65] K. Liu, J. Yang, X. Li et al., "Study on the long-hole raising technique using one blast based on vertical crater retreat multiple deck shots," *International Journal of Rock Mechanics and Mining Sciences*, vol. 109, pp. 52–67, 2018.

[66] K. Liu, X. Li, H. Hao et al., "Study on the raising technique using one blast based on the combination of long-hole presplitting and vertical crater retreat multiple-deck shots," *International Journal of Rock Mechanics and Mining Sciences*, vol. 113, pp. 41–58, 2019.